Title

Techno-Economic Analysis of Solid Oxide Fuel Cell-Gas Turbine Hybrid Systems for Stationary Power Applications Using Renewable Hydrogen

Journal

Energies, 16(13)

ISSN

1996-1073

Authors

Chan, Chun Yin

Rosner, Fabian

Samuelsen, Scott

Publication Date

2023-12-08

DOI

10.3390/en16134955

energies

MDPI

Article

Techno-Economic Analysis of Solid Oxide Fuel Cell-Gas Turbine Hybrid Systems for Stationary Power Applications Using Renewable Hydrogen

Chun Yin Chan [1], Fabian Rosner [1,2,*] and Scott Samuelsen [1]

[1] Advanced Power and Energy Program, University of California, Irvine, CA 92697, USA
[2] Lawrence Berkeley National Laboratory, 1 Cyclotron Rd, Berkeley, CA 94720, USA
* Correspondence: fabianrosner@lbl.gov

Abstract: Solid oxide fuel cell (SOFC)–gas turbine (GT) hybrid systems can produce power at high electrical efficiencies while emitting virtually zero criteria pollutants (e.g., ozone, carbon monoxide, oxides of nitrogen and sulfur, and particulate matters). This study presents new insights into renewable hydrogen (RH_2)-powered SOFC–GT hybrid systems with respect to their system configuration and techno-economic analysis motivated by the need for clean on-demand power. First, three system configurations are thermodynamically assessed: (I) a reference case with no SOFC off-gas recirculation, (II) a case with cathode off-gas recirculation, and (III) a case with anode off-gas recirculation. While these configurations have been studied in isolation, here we provide a detailed performance comparison. Moreover, a techno-economic analysis is conducted to study the economic competitiveness of RH_2-fueled hybrid systems and the economies of scale by offering a comparison to natural gas (NG)-fueled systems. Results show that the case with anode off-gas recirculation, with 68.50%-lower heating value (LHV) at a 10 MW scale, has the highest efficiency among the studied scenarios. When moving from 10 MW to 50 MW, the efficiency increases to 70.22%-LHV. These high efficiency values make SOFC–GT hybrid systems highly attractive in the context of a circular economy as they outcompete most other power generation technologies. The cost-of-electricity (COE) is reduced by about 10% when moving from 10 MW to 50 MW, from USD 1976/kW to USD 1668/kW, respectively. Renewable H_2 is expected to be economically competitive with NG by 2030, when the U.S. Department of Energy's target of USD 1/kg RH_2 is reached.

Keywords: solid oxide fuel cell; SOFC–GT hybrid; anode and cathode recirculation; techno-economics; green hydrogen

Citation: Chan, C.Y.; Rosner, F.; Samuelsen, S. Techno-Economic Analysis of Solid Oxide Fuel Cell-Gas Turbine Hybrid Systems for Stationary Power Applications Using Renewable Hydrogen. *Energies* **2023**, *16*, 4955. https://doi.org/10.3390/en16134955

Academic Editor: David Borge-Diez

Received: 3 June 2023
Revised: 19 June 2023
Accepted: 21 June 2023
Published: 26 June 2023

1. Introduction

The need for reducing greenhouse gas (GHG) and criteria air pollutant (CAP) emissions continues to intensify as CO_2 levels in the atmosphere are rising and degradation of urban air quality increases concern for public health. Consequently, a shift away from traditional power generation technologies is crucial to enable cleaner, more sustainable, and more efficient power generation. Among the power generation technologies, solid oxide fuel cell (SOFC)–gas turbine (GT) hybrid systems stand out as one of the most promising technologies for clean and sustainable power due to their high fuel-to-electricity conversion efficiencies and virtually zero emission of criteria pollutants. These features will allow these systems to play a crucial part in buffering intermittencies from renewables as well as providing baseload power from biomass-based H_2 where high efficiencies help to reduce the feedstock demand. SOFC–GT hybrid systems particularly benefit from the synergistic symbiosis of SOFC and GT technologies, which allows them to reach higher efficiencies than stand-alone SOFC or GT systems [1]. Current SOFCs operate at temperatures between 600 and 1000 °C, which allows the use of high-quality waste heat for cogeneration purposes or a bottoming cycle, leading to higher thermal and/or electrical efficiencies [2]. In

the early 2000s, Siemens Westinghouse Power Corporation introduced and successfully demonstrated a pressurized SOFC–GT hybrid system fueled by natural gas (NG) using a tubular SOFC stack design [3,4]. Instead of relying on a steam generator to adjust the steam-to-carbon ratio, the configuration was based on a recycling scheme, where a portion of the SOFC anode off-gas was mixed with the SOFC fuel via an ejector to allow the system to reach higher efficiencies and reduce capital costs. The hybrid system was rated at 220 kW_e with the SOFC producing 180 kW_e and the GT producing 40 kW_e. Three thousand hours of steady state operation were successfully demonstrated at an operating pressure of around 3 bar while achieving an electrical efficiency of up to 53%-LHV [5].

There are several methods to optimize the performance of SOFC stacks, and one of them is to operate the SOFC under pressurized condition. Although there are challenges related to the pressurization of the SOFC stacks, such as gas sealing, material selection, and thermal management [6], the performance advantages provided by pressurization are significant. Willich et al. [7] investigated the operational behavior of pressurized SOFCs by modeling and experimental validation. Their results show that an increase in pressure increases the power density of the SOFC. For instance, an increase in operating pressure from 1.4 bar to 3 bar increases the power density by 23%. Seidler et al. [8] performed similar studies and concluded that an increase in operating pressure from 1.4 bar to 3 bar results in a 13.8% increase in the SOFC's performance, namely a reduction of overpotentials and an increase in current density.

Additional findings show that an increase in fuel utilization (FU) increases the power output and a decrease in voltage increases the current density, suggesting that higher efficiencies are possible when operating a SOFC at elevated pressures. Gandiglio et al. [9] computationally studied pressurized and atmospheric operating conditions at large scale SOFC power plants in the 230–240 MW range. Their results show that pressurized conditions lead to a reduction in exergy destruction of approximately 20% and a 3% reduction in levelized cost of electricity (LCOE) compared to ambient pressure operating conditions. An investigation of pressure effects upon thermal cell gradients and specific SOFC cost ($/kW) showed that under pressurized condition thermal gradients and specific SOFC cost can be reduced [10].

Although a SOFC alone can reach high efficiencies, integrating it with a GT to form a hybrid system can provide even higher efficiencies [11,12] and solves some of the key problems associated with the low efficiency of GTs and the production of harmful pollutants [13]. In previous work [14], the effect of SOFC operating pressure and cell operating voltage on a SOFC–GT hybrid system's performance and cost-of-electricity (COE) was investigated. Results show that the optimal configuration is to operate the cell at a voltage of 0.82 V, a pressure of 5 bar, and a FU of 85%.

In addition to the SOFC operating pressure, cell voltage and FU, different SOFC recirculation schemes, such as anode recirculation, cathode recirculation, or no recirculation, will affect the hybrid system performance. Wang et al. [15] developed a biogas-fueled SOFC–GT hybrid system employing anode and combustor exhaust recirculation ejectors. The SOFC operates at a FU of 75% and an operating pressure of 3.2 bar. The operating temperature of the SOFC is between 873 and 1123 K, and the thermal gradient is less than 10 K/cm. Their results show that anode recirculation can increase the electrical efficiency of the hybrid system and protect the SOFC from thermal cracks due to a reduction in thermal gradients. Moreover, the recirculation of combustor exhaust gas can reduce the amount of heat rejection and therefore improve the power generation efficiency and overall power output. Furthermore, recirculation allows the system to safely operate in a wider range of temperatures. For optimal power generation efficiency and safety, the recirculation ratio should be kept at 0.4 for anode recirculation and 0.425 for combustor off-gas recirculation. The optimal system is rated at 167 kW with 62.21% efficiency.

Saebea et al. [16] developed two ethanol-fueled SOFC–GT hybrid systems employing no off-gas recirculation and cathode off-gas recirculation. The SOFC operates at a temperature of 1073 K and a FU of 70%. For the base case study (i.e., no recirculation), the

SOFC operating pressure varies from 2 bar to 20 bar. Their results show that the optimal electrical efficiency is 78.27% when operating the SOFC at a pressure of 6 bar. The SOFC produces around 60–75% of the overall system power. For the cathode recirculation case, the recirculation ratio varies from 0 to 0.8 with the SOFC's operating pressure ranging from 2 bar to 8 bar. Their results show that the maximum hybrid system efficiency can be achieved at a cathode off-gas recirculation ratio of 0.3 when the SOFC operates at a pressure between 4 and 6 bar. The study concludes that cathode off-gas recirculation can reduce preheating needs of the SOFC–GT hybrid system by directly utilizing the high temperature cathode exhaust stream.

Chen et al. [17] developed a natural gas (NG)-fueled SOFC–GT hybrid system that employs both anode and cathode recirculation ejectors. The SOFC operates at 0.596 V, 75% FU, and 1073 K. The turbine inlet temperature (TIT) is kept between 1000 and 1200 K, and the SOFC thermal gradient is limited to 10 K/cm. Their results show that reducing the air inlet flowrate while increasing the fuel inlet flowrate will result in more heat generated inside the SOFC due to a faster electrochemical reaction, thus increasing both the anode and cathode outlet temperature. The hybrid system produces a total of 328-kW_e of power at 63% efficiency, which includes 270-kW_e from the SOFC and 58-kW_e from the GT. Cheddie [18] proposes another NG-fueled SOFC–GT hybrid with a net power output of 37 MW_e at 66.2% thermodynamic efficiency. A techno-economic analysis has also been presented and shows that the net present value (NPV) of the power plant is USD 34.9 million, with a SOFC cost of USD 23.8 million and a payback period of 3.3 years.

Most of the SOFC–GT hybrid systems utilize hydrocarbons as fuel, predominately NG. However, these fuels produce CO_2 emissions and will eventually be depleted, making them impractical for a zero-carbon future. As an alternative, hydrogen (H_2) is promising because (i) H_2 has zero carbon emissions [19–22], (ii) H_2 can be produced sustainably and renewably via electrolysis [23,24], (iii) H_2 can be used as energy storage for intermittent renewable resources, and (iv) H_2 costs are rapidly declining [25,26]. Despite the lack of data for H_2-fueld SOFC–GT hybrid systems, the above-mentioned NG-based systems give a good understanding of SOFC–GT hybrid system design considerations.

Chinda et al. [27] propose two H_2-fueled SOFC–GT hybrid systems employing combustor and turbine exhaust recirculation. The first configuration recovers part of the heat from the combustor exhaust with the incoming fuel and then utilizes the heat from the turbine exhaust with the incoming air. Instead of using the combustor exhaust, the second configuration only recovers heat from the turbine exhaust using both fuel and air. The SOFC operates at a pressure of approximately 3 bar. Their results show that the electrical efficiency for the first configuration is 58% with a total power output of 463 kW_e. The electrical efficiency for the second configuration is 53.5% with a power output of 427 kW_e, showing that using combustor and turbine exhaust for heat recovery provides a higher efficiency and power output.

Kuchonthara et al. [28] propose various enhanced H_2-fueled SOFC–GT cycles including a steam injection cycle (SOFC–STIG), a hybrid with bottoming Rankine cycle (SOFC–GT/ST), and a hybrid that is built upon the humid air turbine cycle (SOFC–HAT), all without any off-gas recirculation. In their study, the FU varied from 45% to 95% and the pressure ratio (PR) varied from 5 to 15. The results show that the SOFC–HAT cycle reaches the highest thermal efficiency and specific work. The highest thermal efficiency is 68.22% at a PR of 5 and a FU of 75%. Martinez [29] used a dynamic model to study a H_2-fueled SOFC–GT hybrid for long-haul locomotive application employing a cathode recirculation blower. The cathode recirculation system is shown to improve thermal cell management while maintaining the system's performance without adding much complexity and cost. His results show that the system can reach above 70%-LHV efficiency at start-up while maintaining around 68%-LHV efficiency when approaching steady state.

In summary, SOFC–GT hybrid systems are promising technologies for the future. Most of the literature today focuses on the use of NG or other hydrocarbons as fuels. These studies evaluate the benefits of anode, cathode, and combustor exhaust recirculation

schemes, but techno-economic analyses remain limited. Although H_2 is a promising energy vector for the future, only a limited number of studies have been published on its use as a fuel in SOFC–GT hybrid systems. To the best of the authors' knowledge, until now, no study has examined the differences between anode, cathode, and no recirculation configurations for H_2-fueled SOFC–GT hybrid systems. Moreover, detailed techno-economic analyses of H_2-fueled SOFC–GT hybrid systems are yet to be presented. Against this backdrop, the current study aims to provide a performance evaluation of H_2-fueled SOFC–GT hybrid systems with different off-gas recirculation schemes and provide new techno-economic insights into the utilization of renewable hydrogen (RH_2) in SOFC–GT hybrid systems. To gauge the economic viability of these RH_2-fueled hybrid systems, a comparison to NG-fueled hybrid systems is also presented.

2. Methodology

Stationary hybrid systems of two different sizes, 10 MW and 50 MW, are developed based on steady state process simulations. The simulation results serve as inputs for the techno-economic analysis and are used to establish capital and operating costs. The goal of this work is to investigate three system configurations: (i) no SOFC off-gas recirculation, (ii) cathode off-gas recirculation, and (iii) anode off-gas recirculation. Configurations (ii) and (iii) use an ejector to enable off-gas recirculation without cooling and reheating of the recirculated gas stream. To establish a fair comparison between the different scenarios, operating conditions such as fuel flowrate, SOFC FU, operating temperature, operating pressure, and voltage are held constant throughout the study scenarios. Moreover, the SOFC needs to meet the following thermal constraints: (i) the global temperature difference of the positive-electrode-electrolyte-negative-electrode (PEN) structure is kept below 150 K ($T_{PEN,Max}$–$T_{PEN,Min}$), and (ii) the SOFC local PEN temperature is kept below 15 K/cm. The recuperators are limited to a maximum effectiveness of 90% due to economic considerations.

2.1. Plant Site Characteristics

ISO conditions are used in this study with an ambient air temperature of 15 °C, ambient pressure of 1 atm, and a relative humidity of 60%. Table 1 shows the plant site characteristics and Table 2 shows the plant site air composition.

Table 1. Plant site characteristics.

Parameter	Value	Unit
Elevation	0	M
Barometric Pressure	1	Atm
Design Ambient Temperature	15.0	°C
Design Ambient Relative Humidity	60	%

Table 2. Ambient air composition.

Component	Volume (%)
N_2	77.315
O_2	20.741
H_2O	0.987
Ar	0.924
CO_2	0.033

2.2. Fuel

2.2.1. Renewable Hydrogen Characteristics

The stationary power plants in this study are supplied with RH_2, which is produced by electrolyzers utilizing renewable electricity and water as feedstock. Therefore, it is assumed

that the only "impurity" present in the fuel is water vapor. Typical hydrogen purities from this process are around 99.99% [30,31]. Table 3. shows the composition of the supplied RH_2.

Table 3. Hydrogen composition [30,31].

Component	Mole (%)
Hydrogen	99.99
Water	0.01

The RH_2 is assumed to be distributed using the existing (retrofitted) natural gas pipeline infrastructure, which will be able to provide RH_2 at a pressure of 4.1 bar [32]. Table 4 shows the RH_2 supply pressure and temperature assumptions for this study.

Table 4. Hydrogen supply pressure and temperature [32].

Parameter	Value	Unit
Pressure	4.1	bar
Temperature	15.0	°C

Following the recommendation of Kopasz [33], no odorants are added to the H_2 as odorants might interfere with the fuel cell power generation mechanism. Commercially available H_2 detectors can detect H_2 concentrations 4000 times less than the lower flammability limit. Along with the detectors, features such as automatic shut-off valves and startup of ventilation fans can provide increased levels of safety over that provided by an odorant strategy by removing reliance on individuals to resolve potential problems.

2.2.2. Fuel Cost

This study compares the fuel cost between RH_2 and NG for the hybrid system. The RH_2 obtained via electrolysis is currently not as cost-competitive as other non-renewable hydrogen production methods, including steam methane reforming (SMR) and coal gasification (CG) [34]. However, large-scale deployment of electrolyzers and the development of hydrogen infrastructure will substantially decrease the cost of RH_2 in the coming decades. The US Department of Energy (DOE) seeks to reduce the cost of RH_2 by 80% in the next decade, or USD 1 per 1 kg ("111") [35,36]. Table 5. shows the DOE targets for the cost of hydrogen from electrolysis and NG price projections [37] by taking the average of the available data, which will serve as the fuel cost basis in this study. Current cost reduction of RH_2 production is lagging behind; however, with tax credits available in the US, of up to USD 3/kg, the cost targets for 2023 could be achievable (based on regression fit). With respect to natural gas, prices remain volatile and have experienced an enormous increase in 2022 due to the Ukraine conflict. After a recent decrease in NG prices, currently, US industrial customers pay an average price of USD 5–6/MMBTU which is in good agreement with the predicted trends.

Table 5. Summary of fuel cost basis.

Year	2020	2023	2025	2030
Total RH_2 Cost ($/kg H_2)	5.00	2.96	2.00	1.00
Total NG Cost ($/MMBtu)	4.20	5.86	7.08	8.19

2.2.3. LHV Efficiency

The lower heating value (LHV) efficiency is used to evaluate the hybrid system's performance. The case with the highest LHV efficiency is used for the cost analysis, and the efficiency can be defined as:

$$\varepsilon_{\mathrm{LHV}} = \left(\frac{W_{\mathrm{net}}}{\dot{m}_{\mathrm{H_2}} \mathrm{LHV}_{\mathrm{H_2}}} \right) \cdot 100\% \tag{1}$$

2.3. Solid Oxide Fuel Cell

2.3.1. SOFC Modeling

The SOFC model in this study is adopted from [38], which is a quasi 2D finite volume element model for the electrochemical reaction of H_2. It accounts for the temperature dependence of reaction kinetic, mass transport, and overpotentials and can accurately predict the SOFC performance and contains corrections for the operating pressure. The original model has the additional feature of supporting internal reforming reactions; however, since the fuel in this study is pure H_2, this feature has been disengaged. Throughout this study, the following parameters are held constant: SOFC inlet temperature, SOFC inlet pressure, FU, SOFC voltage, SOFC pressure drop, and heat exchanger pressure drops. The model will determine SOFC air utilization, current density, FU (number of stacks is adjusted to keep FU constant), and outlet temperature (fuel-to-air ratio is adjusted to stay within the thermal limits). Table 6 shows the summary of SOFC parameters.

Table 6. Summary of SOFC parameters.

Constant Parameters	Value	Unit
Inlet Temperature	973	K
Inlet Pressure	5.0	bar
Fuel Utilization	83	%
Stack Voltage	0.82	V
Inverter Losses	2	%
Fuel/Air Channel Length	0.2	m
Fuel/Air Channel Width	0.002	m
Rib Width	0.003	m
Number of Channels	50	-
Fuel Channel Height	0.001	m
Air Channel Height	0.002	m
Overall Height	4.928	mm
Anode Thickness	400	µm
Cathode Thickness	20	µm
Max. Local PEN Temp. Gradient	15	K/cm
Max. Overall PEN Temp. Gradient	150	K
SOFC Heat Loss	0.5	%-LHV

In SOFCs, oxygen ions (O^{2-}) act as the mobile compound because a solid ceramic electrolyte is employed. On the cathode side, O^{2-} is produced when an oxygen molecule reacts with electrons. On the anode side, electrons are produced when a hydrogen molecule reacts with O^{2-}. The electrochemical half reactions on the anode and cathode sides can be written as:

$$\text{Anode}: \ H_2 + O^{2-} \rightarrow H_2O + 2e^- \tag{2}$$

$$\text{Cathode}: \ \frac{1}{2}O_2 + 2e^- \rightarrow O^{2-} \tag{3}$$

The Nernst equation is used to estimate the thermodynamic performance of the SOFC based on the half reactions, which can be written as:

$$E = E^0 + \frac{\Delta \hat{s}}{nF}(T - T_0) - \frac{RT}{nF} \ln\left(\frac{\prod a^{v_i}{}_{\text{Products}}}{\prod a^{v_i}{}_{\text{Reactants}}}\right) \quad (4)$$

where E is the cell potential in V, $\hat{s}$ is the reaction entropy in J/mol-K, n is the number of electrons involved in electrochemical half reactions, F is the Faraday constant, T is the temperature in K, and a is the activity.

Like all fuel cells, SOFCs suffer from three major losses: activation losses (η_{act}), ohmic losses (η_{ohmic}), and concentration losses (η_{conc}) [39–41]. Therefore, these losses need to be subtracted from the ideal voltage (given by the Nernst equation) to determine the actual SOFC operating voltage. The operating voltage can be written as:

$$E_{\text{SOFC}} = E - \eta_{\text{act}} - \eta_{\text{ohmic}} - \eta_{\text{conc}} \quad (5)$$

Activation losses are presented on both the anode and cathode sides of the SOFC due to energy associated with overcoming the activation barrier of the electrochemical half reactions at the catalyst interface, which can be determined by:

$$\eta_{\text{act}} = \eta_{\text{act,a}}(j) + \eta_{\text{act,c}}(j) \quad (6)$$

where $\eta_{\text{act}}(j)$ can be expressed as:

$$\eta_{\text{act}}(j) = \frac{RT}{\alpha nF} \sinh^{-1}\left(\frac{j}{2j_{\text{act}}}\right) \quad (7)$$

where α is the electron transfer coefficient and j_{act} is the electric current density and can be calculated using the Butler–Volmer equation:

$$j_{\text{act}} = j_0\left[\exp\left(\frac{\alpha nF\eta_{\text{act}}}{RT}\right) - \exp\left(-\frac{(1-\alpha)nF\eta_{\text{act}}}{RT}\right)\right] \quad (8)$$

j_0 is the exchange current density, which is:

$$j_{0,\text{a}} = \gamma_{\text{a}}\left(\frac{p_{\text{H}_2}}{p_{\text{ambient}}}\right)\left(\frac{p_{\text{H}_2\text{O}}}{p_{\text{ambient}}}\right)\exp\left(-\frac{E_{\text{A,a}}}{RT}\right) \quad (9)$$

for the anode and:

$$j_{0,\text{c}} = \gamma_c\left(\frac{p_{\text{O}_2}}{p_{\text{ambient}}}\right)^{0.25}\exp\left(-\frac{E_{\text{A,c}}}{RT}\right) \quad (10)$$

for the cathode. Ohmic losses are based on Ohm's law, which are losses due to charge transport inside a conductor. In a SOFC, the majority of ohmic losses come from oxygen ions due to movement through the electrolyte, and electrons contribute to the minority of such losses:

$$\eta_{ohmic} = iR_{\text{ohmic}} = i\left(R_{\text{O}_2} + R_{\text{e}}\right) = i(R_{\text{PEN}} + R_{\text{a}} + R_{\text{c}}) \quad (11)$$

where i is the current in A, R_{PEN} is the positive-electrode–electrolyte–negative-electrode (PEN) electric resistance in Ω, and R_{a} and R_{c} are electric resistance for anode and cathode in Ω, respectively.

Concentration losses are energy losses associated with mass transfer of species from the stack's flow channel to the triple phase boundary (TPB), which are present on both the anode and cathode sides. Although diffusion losses are negligible at low current densities, they can become substantial as species conversion rates increase. Concentration losses

are based on the respective diffusion kinetics on anode and cathode sides, which can be calculated by:

$$\eta_{\text{conc}} = \eta_{\text{conc,a}} + \eta_{\text{conc,c}} = \frac{RT}{2F} \ln\left(\frac{x_{\text{H}_2}\, x_{\text{H}_2\text{O,TPB}}}{x_{\text{H}_2\text{O}}\, x_{\text{H}_2\text{,TPB}}}\right) + \frac{RT}{4F} \ln\left(\frac{x_{\text{O}_2}}{x_{\text{O}_2\text{,TPB}}}\right) \tag{12}$$

where x is mole fraction of species, and x_{TPB} is the mole fraction of species in the triple phase boundary, which can be calculated by:

$$x_{\text{H}_2\text{O,TPB}} = x_{\text{H}_2\text{O}} + \frac{jRT\delta_{\text{a}}}{2Fp_{\text{a}}D_{\text{a}}} \tag{13}$$

$$x_{\text{H}_2\text{,TPB}} = x_{\text{H}_2} - \frac{jRT\delta_{\text{a}}}{2Fp_{\text{a}}D_{\text{a}}} \tag{14}$$

$$x_{\text{O}_2\text{,TPB}} = x_{\text{O}_2} - \frac{jRT\delta_{\text{c}}}{4Fp_{\text{c}}D_{\text{c}}} \tag{15}$$

where δ is the thickness in m and D is the effective diffusivity in m^2/s.

2.3.2. SOFC Cost

The SOFC cost basis is based upon a SOFC manufacturing analysis conducted by the Battelle Memorial Institute [42]. The relevant production scale used for this study is 1000 units per year. Different stack components and process steps, such as assembly, welding, and sealing frame, contribute to the stack cost. Each of these components and process steps incorporate costs for materials, machines, labor, scrap, and tooling.

Hastelloy X is the material used for the two end plates of every stack, and ferritic steel sheet is used for the interconnects. The anode support is produced via tape casting of yttria-stabilized zirconia (YSZ) and nickel oxide (NiO) slurry. The cathode material is made of lanthanum strontium cobalt ferrite (LSCF), and the contact layer is made of lanthanum strontium manganite (LSM) and YSZ. The cost of the stack is calculated based on the physical parameters as provided in Table 6 and the above-mentioned individual cost items.

2.4. Gas Turbine

2.4.1. GT Parameters

Based on the literature discussed above, the SOFC in the hybrid system produces most of the power and the GT is responsible for controlling the air flowrate for the SOFC's thermal management while producing additional power. The GT modeled in this work is based on a commercial 1.8 MW engine, which can supply enough pressurized air for a hybrid system of approximately 10 MW. The component efficiencies have been calibrated using available engine data. The GT mechanical losses are mainly associated with generator and bearing losses. The combustor pressure drop is assumed to be 4%, and the heat loss is assumed to be 1%-LHV. In the 50 MW plant, the GT is upgraded to a larger engine with slightly higher efficiency. Table 7 shows a summary of the GT parameters.

Table 7. Summary of GT parameters.

10 MW GT Operational Parameters	Value	Unit
Compressor Polytropic Efficiency	84.85	%
Expander Polytropic Efficiency	83.31	%
50 MW GT Operational Parameters	Value	Unit
Compressor Polytropic Efficiency	85.60	%
Expander Polytropic Efficiency	85.70	%
Other Operational Parameters	Value	Unit
Combustor Pressure Drop	4	%
Combustor Heat Loss	1	%-LHV

2.4.2. GT Cost

The cost of an *n*-th plant GT for this hybrid system can be estimated using the following correlation [43]:

$$C_{GT} = 0.1391\left(\dot{m}_a\right)^{0.73} + 0.0474\left(\dot{m}_a\right)^{0.73}(PR)^{0.55} + 8.8221\left(10^{-13}\right)\left(\dot{m}_a\right)^{0.73}(TIT)^{3.50} + 0.0356 \quad (16)$$

where C_{GT} represents the GT cost in million USD, $\dot{m}_a$ represents the air flowrate in kg/s, PR represents the pressure ratio, and TIT represents the turbine inlet temperature in K.

2.5. Other Equipment

2.5.1. Ejector

A fuel ejector is used in this study to recirculate the anode-off gas and cathode-off gas streams. The higher-pressure stream (i.e., inlet fuel or air stream) entrains the lower-pressure stream (i.e., anode or cathode recycle stream) in the suction chamber. After mixing the two streams, kinetic energy is converted into static pressure in the diffuser section of the ejector. The ejector model in this study is developed based on the recommendation provided by Eeden et al. [44], which provides accuracy of the ejector's efficiency within the range of ±2%.

2.5.2. Heat Exchanger

This study utilizes two types of heat exchangers: recuperators and intercoolers. Recuperators are used in all three cases to recover the GT exhaust heat with the incoming fuel and air. An intercooler is used only in the anode recirculation case to reduce the amount of fuel compressor work. The heat exchanger design follows the recommendation provided by [45], which is specific for high temperature fuel cell systems. All heat exchangers are limited to 90% effectiveness to keep the plant economically efficient.

2.5.3. Fuel Compressors

The fuel compressors in this study are rotary screw compressors, to minimize pressure fluctuations/pulsating, which are needed to increase the inlet fuel pressure before the fuel enters the ejector and heat exchangers. The polytropic efficiency is estimated with 70%.

2.6. Techno-Economic Basis

The cost components of this study include total plant cost (TPC), annual fixed operating cost (AFOC), annual variable operating cost (AVOC), and the resulting cost of electricity (COE). According to DOE's techno-economic analysis of fuel cell systems [46], the expected accuracy of this methodology ranges from minus 15% to plus 30%.

2.6.1. Total Plant Cost Basis

The TPC accounts for the process equipment and supporting facilities, direct and indirect labor, engineering procurement and construction (EPC) services, process and project

contingencies, and auxiliary plant equipment such as accessory electric plant equipment, instrumentation and controls, improvement to site, and buildings and structures. The scaled equipment cost can be determined via [47]:

$$C_{eq} = C_r \left(\frac{k}{k_r}\right)^u \left(\frac{n}{n_r}\right)^{0.9} \quad (17)$$

where C_{eq} represents the equipment cost in USD, C_r represents the reference cost in \$USD, k represents the scaled parameter, k_r represents the reference parameter, u represents the scaling exponent, n represents the number of trains for the scaled plant, and n_r represents the number of trains for the reference plant.

A scaling equation can be used to escalate the cost to the present year if the reported cost is from earlier year, which is given by [48]:

$$C_p = C_r(1+r)^{t-t_0} \quad (18)$$

where C_p is the present cost, C_r is the reference cost, r is the annual escalation rate (assumed to be 3% in this study), t is the scaled year, and t_0 is the reference year.

2.6.2. Annual Fixed Operating Cost Basis

The annual fixed operating cost (AFOC) includes expenses such as operating labor, maintenance labor, and administrative and support labor, as well as property tax and insurance. Maintenance labor is assumed to be 35% of the total maintenance cost [49], which is estimated based on component-specific maintenance factors. Administrative and support labor are approximated using 25% of the operating and maintenance labor costs, and tax and insurance account for 2% of the TPC [49]. To operate the plant, two skilled operators are needed during each shift. Table 8 summarizes the labor rate and the labor burden

Table 8. Annual fixed operating cost basis [49].

Cost Basis Parameters	Value
Operating Labor Rate	USD 40.85/h
Operating Labor Burden	30% of Base
Labor Overhead Charge Rate	25% of Labor

2.6.3. Annual Variable Operating Cost Basis

The annual variable operating cost (AVOC) is another annual cost in addition to the AFOC. The AVOC includes fuel cost, stack replacement cost, and maintenance cost. The fuel cost in this study is the cost of RH_2, which has been described earlier. The stack replacement cost accounts for the cost to replace a fuel cell stack and it is assumed that the used stacks will be returned to the manufacturer after reaching their end-of-life at no additional cost for resource recovery. The maintenance cost is the cost associated with operating and maintaining the system.

2.6.4. Cost of Electricity (COE) Basis

The first year cost of electricity (COE) in this study is calculated by [14,47]:

$$C_{COE} = \frac{f_{CCF}C_{TOC} + C_{AFOC} + f_{CF}C_{AVOC}}{f_{CF}MWh} \quad (19)$$

where C_{COE} represents the levelized COE in the first year (USD/MWh), f_{CCF} represents the capital charge factor, C_{TOC} represents the total overnight capital (USD), including the TPC, land cost, pre-production cost, and other owner expenses, C_{AFOC} represents the annual fixed operating cost (USD), C_{AVOC} represents the annual variable operating cost (USD) at

full capacity, f_{CF} represents the capacity factor (assumed to be 90% in this study) of the plant, and *MWh* represents the annual net megawatt hours at 100% capacity.

3. Results and Discussion

Three cases are used to evaluate the thermodynamic performance of the 10 MW hybrid system, including a base case with no recirculation, a cathode off-gas recirculation case, and an anode off-gas recirculation case. The case with the best thermodynamic performance (i.e., highest efficiency and power output) will be used to further investigate the hybrid performance at a 50 MW scale. A detailed description for the constant SOFC and GT parameters are listed in Tables 6 and 7.

3.1. Hybrid System Configurations

3.1.1. Base Configuration

The base configuration is the simplest configuration and does not use any SOFC off-gas recirculation. In this design, ambient air is compressed in the GT compressor and pre-heated against the GT exhaust gas (as much as possible at 90% exchanger effectiveness) as well as the SOFC cathode off-gas to reach a SOFC inlet temperature of 700 °C. To reach the SOFC inlet pressure of 5 bar on the fuel side, the incoming RH_2 needs to be compressed. After compression, the fuel is pre-heated to 700 °C using the GT exhaust downstream of the air pre-heater and the anode off-gas. Maximizing GT exhaust recuperation is ideal as it decreases the GT exhaust temperature and therefore the amount of heat rejection, leading to an increase in overall cycle efficiency. The off-gases from the anode, which still contains unutilized fuel, as well as the cathode off-gas, which still contains unutilized oxygen, are combined in an oxidizer to increase the temperature of the working fluid before it enters the GT expander. The top of Figure 1 shows the base configuration, and Table A1 presents the corresponding state-point stream data.

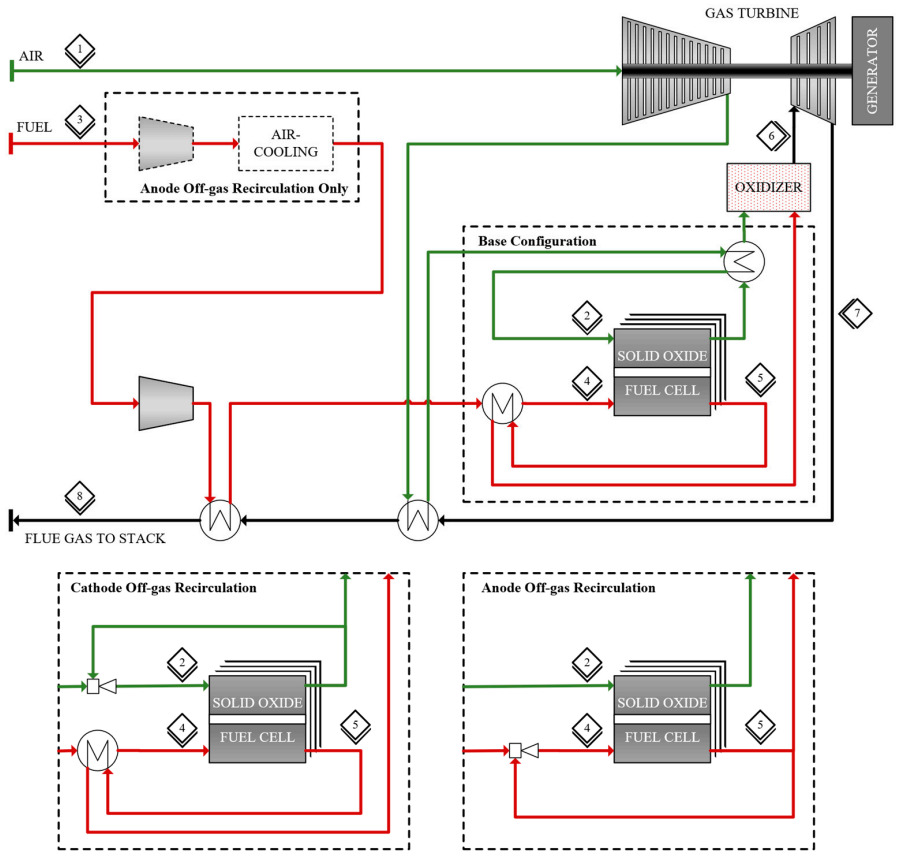

Figure 1. Hybrid system configurations for base configuration (**top**), cathode off-gas recirculation (**bottom left**), and anode off-gas recirculation (**bottom right**).

3.1.2. Cathode Off-Gas Recirculation

In the cathode off-gas recirculation case, an ejector is placed upstream of the SOFC air inlet. The ejector uses partially pre-heated higher-pressure primary air from the GT compressor and the high-temperature lower-pressure cathode off-gas. The cathode feed enters the SOFC with an inlet temperature of 700 °C and an inlet pressure of 5 bar. The amount of cathode off-gas recirculation is based upon the amount of heat required to preheat the air coming from the GT exhaust gas recuperator. In order to facilitate the cathode off-gas recirculation, the GT compressor discharge pressure needs to be increased in order to accommodate the recycle. The bottom left of Figure 1 illustrates the cathode ejector case configuration. The corresponding state-point stream data can be found in the Table A2.

3.1.3. Anode Off-Gas Recirculation

The anode off-gas recirculation case uses an ejector to recycle some of the anode off-gas back to the SOFC anode inlet. In this scenario, the fuel heater that utilizes the anode off-gas can be eliminated. Since the ejector requires sufficiently high pressure, the fuel compression is configured as a 2-stage compression system with an air-cooled intercooler to reduce the compression power. Furthermore, this scenario does not require the cathode off-gas recuperator as the GT exhaust can provide enough heat to completely pre-heat the cathode air. The bottom right of Figure 1 depicts the configuration of the anode off-gas recirculation case. The corresponding state-point stream data can be found in the Table A3.

3.2. Thermodynamic Performance

3.2.1. Base Configuration Analysis

The electrical efficiency of the base case is 64.39%-LHV and the total net power output is 9.40 MW_{AC}, with 7.96 MW_{DC} produced by the SOFC and 1.90 MW_{AC} produced by the GT. The power produced by the SOFC is in direct-current (DC) power and the power produced by the GT is in alternating-current (AC) power. The SOFC's DC power is converted to AC power for transmission purposes through an inverter, which accounts for 2% losses. The resulting AC SOFC efficiency is 64.27%-LHV. In this base configuration, the SOFC has 113 stacks, which operate at a FU of 83% and an air utilization (AU) of 22% leading to an average current density of 6862 A/m^2. The maximum local PEN temperature gradient is 13 K/cm, and the maximum global PEN temperature difference is 150 K (limiting factor). To prevent the SOFC from overheating, the GT supplies air at a rate of 58,120 kg/h. After the combustor, the TIT in the GT reaches a temperature of 1125 K. Downstream of the expander the GT exhaust temperature is reduced to 844 K.

In this configuration, the GT reaches an efficiency of 77.26%-LHV which is surprisingly high compared to typical GTs of that size which reach efficiencies of around 28%-LHV under ISO conditions. The reason for this exceptionally high GT efficiency is based on the fact that the definition of efficiency only accounts for the chemical energy in the fuel [50]. In a SOFC–GT hybrid, the GT fuel has a lower heating value of only 266 kJ/kg, and fuel and oxidant enter the combustor in a "pre-heated" state as they are the hot off-gases from the SOFC. This "free" heat/energy from the SOFC can be utilized in the GT expander and boosts the GT efficiency. Downstream of the GT more heat is recovered via recuperators and the flue gas stack temperature is 548 K. The auxiliary plant power consumption is mainly fuel compression with 0.26 MW_e. Other plant equipment accounts for 0.20 MW_e. A summary of the performance results can be found in Table 9 (left column).

Table 9. Comparison of results for 10 MW RH_2-fueled SOFC–GT hybrid.

Overall Performance	Base Case	Cathode Ejector	Anode Ejector
Power Output (MW_{AC})	9.40	9.64	10.00
LHV Electrical Efficiency (%)	64.39	65.98	68.52
SOFC			
Power Output (MW_{DC})	7.96	7.96	7.94
Number of Stacks	113	115	150
Inlet Temperature (K)	973	973	973
Outlet Temperature (K)	1189	1197	1215
Operating Pressure (bar)	5.00	5.00	5.00
Fuel Flowrate (kg/h)	439	439	439
Overall Fuel Utilization (%)	83	83	83
Overall Air Utilization (%)	22	28	30
Max Local PEN Temperature (K/cm)	13	13	14
Max Global PEN Temperature (K)	150	150	150
Average Current Density (A/m^2)	6862	6741	5156
Inverter Losses (%)	2	2	2
GT			
Power Output (MW_{AC})	1.90	2.15	2.62
Air Flowrate (kg/h)	58,120	45,000	42,500
Turbine Inlet Temperature (K)	1125	1342	1376
Turbine Exhaust Temperature (K)	844	1016	1031
Auxiliary Equipment			
Fuel Compressor (MW_e)	0.26	0.26	0.35
Other Auxiliary Load (MW_e)	0.20	0.20	0.21
Exhaust			
Flue Gas Temperature (K)	548	603	585
Flue Gas Flowrate (kg/h)	58,559	45,439	42,940

3.2.2. Cathode Off-Gas Recirculation Analysis

The electrical efficiency of the cathode ejector case is 65.98%-LHV, which is 1.59%-points higher than the base case. The net power output is 9.64 MW_{AC}, essentially the same SOFC power output as in the base case, and a 13% higher GT power output than in the base case. The SOFC power output is not expected to change since the operating voltage and FU are held constant. In order to understand this increase in GT power output, we need to look at the SOFC operation. In the cathode off-gas recirculation case, the GT air flowrate reduces by about 23% as compared to the base case. By using an ejector, oxygen depleted air is recycled back to the SOFC inlet reducing the oxygen concentration at the SOFC inlet, and thus, the chemical potential difference between anode and cathode when compared to the base case. This lower chemical potential difference between anode and cathode is associated with lower reaction rates, and ultimately leads to lower thermal gradients. Thus, less cooling air is needed for the SOFC under constant fuel flow conditions. This increase in air utilization, or fuel-to-air ratio, results in a higher adiabatic flame temperature of the mixture which translates to a higher firing temperature in the GT. The TIT and the GT exhaust temperature in the cathode ejector case are 20% higher compared to the base case, which means that the GT in the cathode off-gas recirculation case is operating more efficiently.

The GT efficiency in this case is 86.59%, which is 9.33% points higher compared to the base case driven by this TIT increase and an increase in SOFC off-gas temperatures. Another way to look at it is to compare the heat rejected through the flue gas. A higher amount of heat rejection indicates a reduction of electrical efficiency. In this case, the flue gas exhaust temperature is 603 K, which is about 10% higher than the base case. However, the 22% reduction in flue gas flowrate as compared to the base case more than offsets the higher temperature, indicating a lower amount of heat rejection to the atmosphere, and thus leading to a higher electrical efficiency. The maximum local and global PEN temperature gradients are identical compared to the base case. There is a 2% increase in SOFC stack

numbers due to a 2% decrease in the average current density as compared to the base case. These numbers are very similar to the base case due to two counter acting effects. The reduced cooling air mass flow leads to an increase of the average PEN temperature (while maintaining the same thermal gradients) accelerating the electrochemical reaction kinetics, especially the oxygen diffusion which is the man resistance. However, at the same time, the lower O_2 concentration on the cathode reduces reaction kinetics at the cathode–electrolyte interface, which leads to a decrease of the oxygen at the anode–electrolyte interface [51]. With concentration effects being slightly more dominant, this leads to a lower current density, and thus, slightly more stacks are needed. The auxiliary loads of the plant remain essentially constant with a fuel compression power of 0.26 MW_e and other auxiliaries of 0.20 MW_e. The middle column of Table 9 provides a summary of the cathode ejector configuration results.

3.2.3. Anode Off-Gas Recirculation Analysis

The electrical efficiency of the anode ejector case is 68.52%-LHV, which is 2.54% points higher than the cathode ejector case and 4.13% points higher than the base case. The net power output is 10.00 MW_{AC}; as the SOFC voltage and FU do not change, the SOFC power remains essentially constant. The higher GT power output is a result of the increased GT efficiency which in the anode off-gas recirculation case is 105.02%, the highest among the studied scenarios. Again, this efficiency is possible because of the "free" heat/energy input from the SOFC off-gas which is not accounted for in the standard LHV definition of efficiency. In order to understand this behavior, we have to look at the SOFC operation. Anode off-gas recirculation recycles reaction products back to the SOFC inlet reducing the fuel concentration, and thus, the chemical potential difference. The slower reaction rates associated with lower fuel concentrations lead to a reduction in cell air-cooling requirement. Similar to the cathode recirculation case, this reduced air-cooling requirement leads to an increase in the TIT and a higher GT efficiency. In the anode recirculation case, this increase in fuel-to-air ratio is more pronounced compared to the cathode recirculation case, which makes it the best performing case among the studied scenarios. The downside of this effect is a significant reduction in current density and increase in required cell stacks despite the fact that the average PEN temperature is the highest among the studied scenarios which in general helps with reaction kinetics.

The anode off-gas recirculation case also has the highest GT exhaust temperature and is able to recover enough heat from the GT exhaust gas to completely preheat the air to the desired SOFC inlet temperature as well as the fuel. Although the flue gas temperature after heat recuperation in the anode ejector case is around 6% higher than the base case, the 27% reduction of flue gas flowrate in the anode ejector case more than offsets the higher temperature, indicating the lowest amount of heat rejection to the atmosphere and thus the highest efficiency and power output. The cathode off-gas recirculation has lower efficiency compared to the anode off-gas recirculation because the former suffers from a lower SOFC off gas temperature, lower TIT, and larger pressure drop associated with the SOFC cathode ejector, which increases the air compression power by 268 kW. In comparison, the extra fuel compression power is only 87 kW. Other plant equipment accounts for 0.21 MW_e. Since the anode ejector case yielded the highest power output and efficiency, the 50 MW scale is built based on the anode off-gas recirculation case. A summary of results is presented in Table 9.

3.2.4. 50 MW Anode Off-Gas Recirculation Performance

The electrical efficiency of the 50 MW anode ejector case is 70.22%-LHV, which is 1.70% points higher than the 10 MW anode ejector case. The GT and fuel compression equipment in the 50 MW case has a slightly higher efficiency compared to the 10 MW case due to equipment scaling effects seen in compressors. In this case, the SOFC produces more than 73.7% of the power, with the remaining 26.3% produced by the GT. Table 10 shows the summary of the thermodynamic performance results for the 50 MW SOFC–GT

hybrid using anode off-gas recirculation. The other auxiliary plant equipment accounts for 1.01 MW_e.

Table 10. Anode ejector case results for 50 MW RH_2-fueled SOFC–GT hybrid.

Overall Performance	Anode Ejector
Power Output (MW_{AC})	50.24
LHV Electrical Efficiency (%)	70.22
SOFC	
Power Output (MW_{DC})	38.99
Number of Stacks	736
Inlet Temperature (K)	973
Outlet Temperature (K)	1217
Operating Pressure (bar)	5.00
Fuel Flowrate (kg/h)	2158
Overall Fuel Utilization (%)	83
Overall Air Utilization (%)	30
Max Local PEN Temperature (K/cm)	14
Max Global PEN Temperature (K)	150
Average Current Density (A/m^2)	5163
Inverter Losses (%)	2
GT	
Power Output (MW_{AC})	13.90
Air Flowrate (kg/h)	206,019
Turbine Inlet Temperature (K)	1382
Turbine Exhaust Temperature (K)	1027
Auxiliary Equipment	
Fuel Compressor (MW_e)	1.64
Other Auxiliary Load (MW_e)	1.01
Exhaust	
Flue Gas Temperature (K)	579
Flue Gas Flowrate (kg/h)	208,175

3.3. Techno-Economic Analysis

After identifying the anode recirculation case as the thermodynamically most favorable configuration, an economic analysis is conducted to gauge its competitiveness in the energy market. The cost analysis provides key economic performance metrics, such as specific plant cost and cost-of-electricity, for a *n*-th plant SOFC–GT hybrid system fueled by RH_2. Furthermore, the RH_2 system is compared to a NG-fueled SOFC–GT hybrid considering pre-pandemic 2020 fuel costs as well as price projection for the years 2025 and 2030. The analysis is conducted in real 2020 USD.

The TPC of the 10 MW SOFC-GT hybrid with anode off-gas recirculation is USD 19,755,000, which leads to a specific plant cost of 1976 USD/kW. The largest cost is the SOFC island with USD 10,745,000 (54.4%) which includes the stacks, power conditioning equipment, housing, and installation. The GT Island contributes, with USD 4,195,000, 21.2% to the TPC while generating about 24.8% of the total power. Other major cost categories are the gas processing, which includes fuel compressors, intercoolers, and flue gas stack system (USD 687,000), heat recuperation for fuel and air heating (USD 1,496,000), and the auxiliary plant equipment, such as electric plant accessory, instrumentation, controls, site improvement, and buildings (USD 2,632,000). A breakdown of the major TPC categories is shown on the top of Figure 2. Considering preproduction costs, inventory capital costs, and other owner's costs, the total overnight capital cost amounts to USD 25,139,000. The fixed operating costs are annual expenses that are not directly coupled to the operation of the plant. Fixed operating costs for the 10 MW plant are USD 2,048,000 on an annual basis.

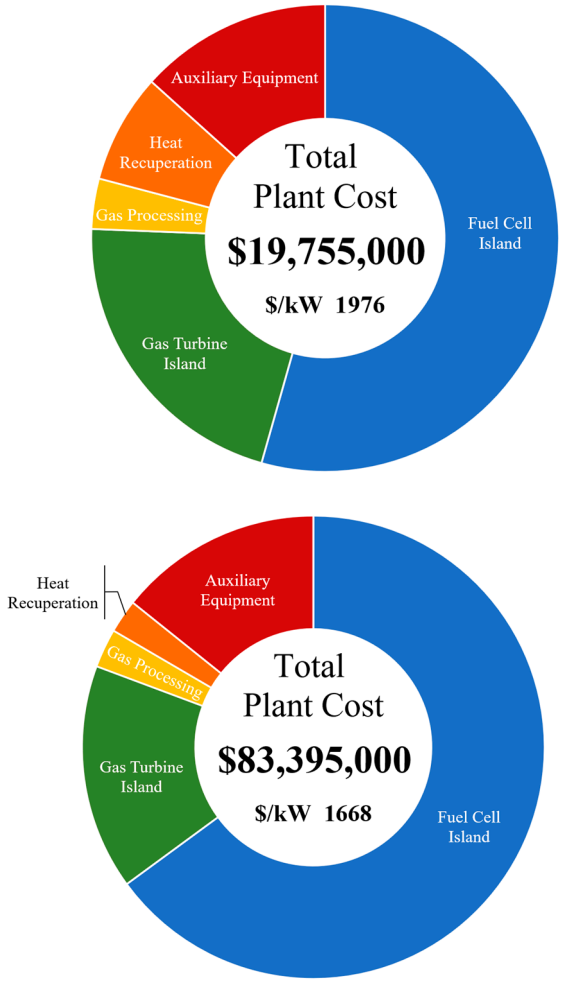

Figure 2. Distribution of TPC for 10 MW (**top**) and 50 MW (**bottom**) RH_2-fueled SOFC–GT hybrid systems.

The largest contributor to the fixed operating costs is the actual operating labor (two operators per shift) with USD 1,163,000. Maintenance labor is USD 159,000 and administrative and support labor is USD 331,000 on an annual basis. Tax and insurance account for USD 395,000 per year. Variable operating costs on the other hand are costs that directly originate from the operation of the plant, such as fuel costs. Using a USD 5.00 per kg of H_2 price, the annual fuel cost is USD 17,317,000, which accounts for 97.6% of the variable operating costs. Other smaller variable operating costs are maintenance materials (USD 266,000 per year) and the levelized fuel cell stack replacement (USD 161,000 per year), which is based on first order 0.002% per 1000 h degradation rate. The resulting cost-of-electricity (COE) for a hybrid system running on RH_2 in the year 2020 is 274.64 USD/MWh.

When moving from 10 MW to a 50 MW scale, the TPC increases by a factor of 4.2 (less than 5.0 due to the economics of scale as described by Equation (17)) to USD 83,395,000. However, due to the modular nature of fuel cells, cost savings related to the SOFC island are small leading to an increase in the relative cost contribution of the SOFC island as seen on the bottom of Figure 2. In the 50 MW plant, the SOFC island accounts for USD 54,157,000, representing 64.9% of the TPC. In the 50 MW plant, the GT is upgraded to a larger engine with slightly higher efficiency, increasing the relative GT power output to 26.3%. At the same time the GT cost on a USD/kW basis is reduced due to the economies of scale and the GT island accounts for only 15.7% of the TPC, or USD 13,133,000. The costs for the other major plant areas are gas processing with USD 2,264,000, heat recuperation with USD 1,954,000, and auxiliary plant equipment with USD 11,887,000. The total overnight capital cost in the 50 MW case, after accounting for preproduction costs, inventory capital costs, and other owner's costs, is USD 104,078,000. For both the 10 MW and the 50 MW plant,

the same number of operators is assumed, since the plant complexity is not increasing, which leads to a substantial reduction in fixed operating costs on a USD/MWh basis. The maintenance costs are USD 622,000 per year, the administrative and support labor is USD 446,000 per year, and the annual tax and insurance costs are USD 1,668,000, leading to a total fixed operating costs of USD 3,899,000 per year. The variable costs are again dominated by the fuel costs which are USD 84,735,000 per year in the year 2020. Levelized stack replacement and maintenance material costs are USD 1,824,000. The resulting COE for the 50 MW hybrid system running on RH_2 in the year 2020 is 249.01 USD/MWh.

At current RH_2 production scales, converting RH_2 back to electricity is comparatively expensive due to the high RH_2 production costs, which are the major cost driving factor for the COE in 2020. On the 10 MW scale, 80% of the COE are fuel costs, and for the 50 MW scenario, over 86% of the COE are fuel costs. In comparison, an equivalent NG-fueled SOFC–GT hybrid in the year 2020 can produce electricity for 82.45 USD/MWh on a 10 MW scale or 60.01 USD/MWh on a 50 MW scale. However, the NG-powered plants emit 269 kg_{CO2}/MWh while the RH_2 plants have zero CO_2 emission. Thus, based on 2020 economics, a CO_2-emission tax of 713 USD/metric ton of CO_2 emitted and 701 USD/metric ton of CO_2 emitted would be necessary to make the 10 MW and 50 MW RH_2 case competitive with the NG case.

By the year 2025, the cost of RH_2 is expected to drop significantly while at the same time the cost for NG is expected to increase. For the year 2025, the projected COE for the RH_2-fueled hybrids are 130.53 USD/MWh (10 MW scale) and 107.99 USD/MWh (50 MW scale). For the same year, the projected NG hybrid COEs are 91.11 USD/MWh (10 MW scale) and 68.66 USD/MWh (50 MW scale), and a CO_2 tax of USD 112 per metric ton of CO_2 emitted is needed, in both cases. When RH_2 reaches the DOE target of 1.00 USD/kg, which is expected for the year 2030, the COE for the RH_2-fueled hybrid systems is expected to fall to 87.36 USD/MWh (10 MW scale) and 65.73 USD/MWh (50 MW scale). By this time, RH_2 will be able to economically outperform NG-fueled hybrid systems without any need for a carbon tax. The COEs of the NG-fueled hybrid systems are expected to slightly decrease after the year 2025; however, with 91.05 USD/MWh (10 MW scale) and 68.60 USD/MWh (50 MW scale), these plants are still more expensive than their renewable counterparts. Figures 3 and 4 show the COE comparison for the RH_2 and NG hybrid systems for the years 2020, 2025, and 2030 for the 10 MW and 50 MW, respectively.

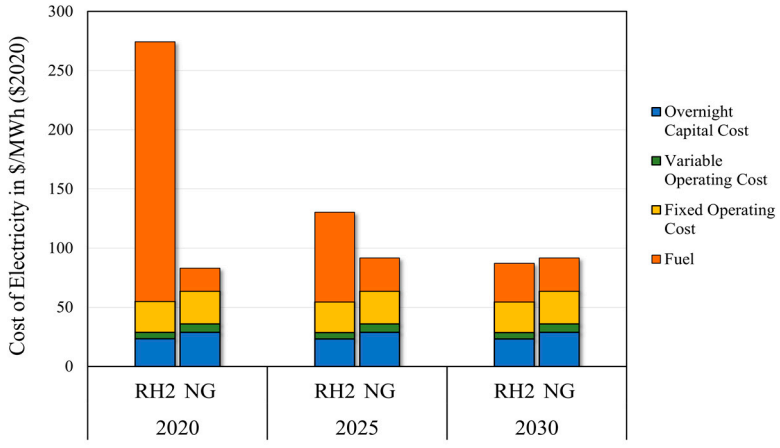

Figure 3. Cost-of-electricity comparison for 10 MW RH_2-fueled and NG-fueled SOFC–GT systems in 2020, 2025, and 2030.

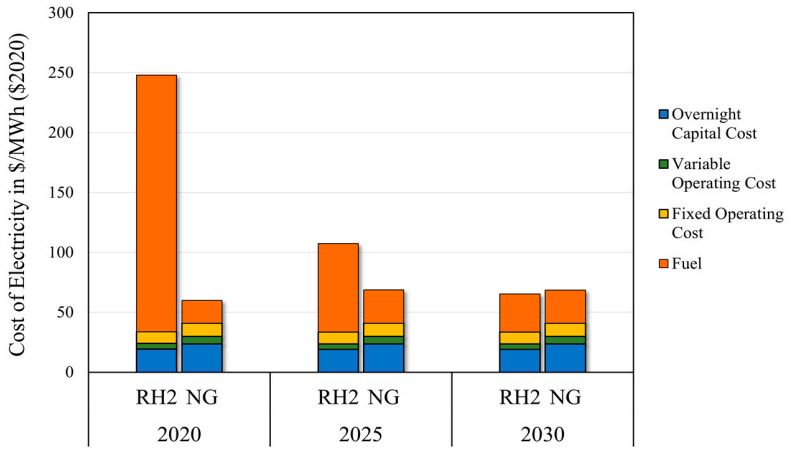

Figure 4. Cost-of-electricity comparison for 50 MW RH_2-fueled and NG-fueled SOFC–GT systems in 2020, 2025, and 2030.

4. Conclusions

SOFC–GT hybrid technology is a promising continuous power generation technology that can produce electric power with ultra-high efficiencies, and virtually zero emission of criteria pollutants. Many research papers employ natural gas for the SOFC–GT hybrid systems, and most focus on the reformation strategy, SOFC operating pressure, and recirculation technique. In this research, the authors present for the first time a comparison of various off-gas recirculation schemes for RH_2 and a detailed economic analysis of when RH_2 will become a viable option for electricity generation.

A screening analysis was first performed on the 10 MW stationary SOFC–GT hybrid using no SOFC off-gas recirculation, cathode off-gas recirculation, and anode off-gas recirculation. The anode off-gas recirculation using an ejector is determined to be the most desirable configuration with the highest efficiency. This configuration has been used to investigate its performance at a larger 50 MW scale including the economies of scale. The 10 MW hybrid reaches an efficiency of 68.52%-lower heating value (LHV), while on a 50 MW scale, an efficiency of 70.22%-LHV is possible. Although SOFCs are modular and cost do not scale well with plant size, savings in traditional balance-of-plant equipment and plant operation labor lead to a substantial reduction in cost-of-electricity. The COE for the 10 MW hybrid is reduced from USD 274.64/MWh to USD 249.01/MWh, or 9%, when moving to a 50 MW scale. Considering price projections for RH_2 and NG, the COE for the 10 MW hybrid is expected to reduce to USD 130.53/MWh in 2025, and to USD 107.99/MWh in 2025 when moving to a 50 MW scale, which is a reduction of 52% and 61%, respectively. Although NG-fueled hybrid systems are more cost competitive until 2025, RH_2-fueled hybrid systems are expected to be cost-competitive by 2030, at both the 10 MW and 50 MW scale. By 2030, the COE of H_2-fueled systems is expected to decrease to USD 87.36/MWh for the 10 MW scale, which is 68% reduction compared to 2020. For the 50 MW scale, the COE is expected to decrease to USD 65.73/MWh, which is about 4–5% lower compared to NG-fueled systems in that year. The results reveal promise for economically viable implementation. Operating SOFC–GT hybrids with anode recirculation is recommended for best electrical efficiency/power output, and thus has the lowest environmental impact. A reduction in renewable H_2 cost is required to enable H_2 as a fuel for distributed generation. Future studies could further explore implications of the various operating modes upon the surge margin when using commercial gas turbine engines in off-design mode or dynamic demand driven operations.

Author Contributions: Conceptualization, C.Y.C. and F.R.; methodology, C.Y.C. and F.R.; software, C.Y.C.; validation, C.Y.C.; formal analysis, C.Y.C. and F.R.; investigation, C.Y.C. and F.R.; writing—original draft preparation, C.Y.C. and F.R.; writing—review and editing, C.Y.C., F.R. and S.S.; visualization, F.R.; supervision, F.R. and S.S.; project administration, S.S.; funding acquisition, S.S. All authors have read and agreed to the published version of the manuscript.

Funding: This research was funded by the U.S. Department of Energy U.S./China Clean Energy Research Center under grant number DE-IA0000018, and the South Coast Air Quality Management District under grant number 19191.

Institutional Review Board Statement: Not applicable.

Informed Consent Statement: Not applicable.

Data Availability Statement: Data sharing not applicable.

Acknowledgments: The authors wish to acknowledge South Coast Air Quality Management District (SCAQMD) and U.S./China Clean Energy Research Center for Water-Energy Technologies under whose sponsorship this work was conducted by the University of California, Irvine. Neither the U.S. Government nor any agency thereof, nor any of their employees, makes any warranty, express or implied, or assumes any legal liability or responsibility for the accuracy, completeness, or usefulness of any information, apparatus, product, or process disclosed, or represents that its use would not infringe privately owned rights. Reference herein to any specific commercial product, process, or service by trade name, trademark, manufacturer, or otherwise does not necessarily constitute or imply its endorsement, recommendation, or favoring by the U.S. Government or any agency thereof. The views and opinions of authors expressed herein do not necessarily state or reflect those of the U.S. Government or any agency thereof.

Conflicts of Interest: The authors declare no conflict of interest.

Nomenclature

Symbols

η_{act}	Activation Losses in V
a	Activity
$\dot{m}_a$	Air flowrate in kg/s
r	Annual Escalation Rate
C_{AFOC}	Annual Fixed Operating Cost in $
MWh	Annual Net Megawatt Hours
C_{AVOC}	Annual Variable Operating Cost in $
f_{CF}	Capacity Factor
f_{CCF}	Capital Charge Factor
$\Delta\hat{s}$	Change in Standard Entropy in J/K
η_{conc}	Concentration Losses in V
C_{GT}	Cost of Gas Turbine in Million USD
D	Effective Diffusivity in m^2/s
j_{act}	Electric Current Density in A/m^2
E_{SOFC}	Electric Potential of SOFC in V
α	Electron Transfer Coefficient
C_{eq}	Equipment Cost in $
j_0	Exchange Current Density in A/m^2
F	Faraday's Constant in C/mol
C_{COE}	Levelized cost of electricity in first year in $/MWh
ε_{LHV}	LHV efficiency in %
LHV_{H_2}	Lower Heating Value of H_2 in J/kg
$\dot{m}_{H_2}$	Mass flowrate of H_2 in kg/s
x	Mole Fraction of Species
n	Moles of Electrons
W_{net}	Net Power Output of the hybrid system in W

n_r	Number of Trains for the Reference Plant
n	Number of Trains for the Scaled Plant
η_{ohmic}	Ohmic Losses in V
O^{2-}	Oxygen Ions
γ	Pre-exponential Factor Exchange Current Density
C_p	Present Cost in $
p	Pressure in bar
E	Reduction Potential in V
C_r	Reference Cost in $
k_r	Reference Parameter
T_0	Reference Temperature in K
t_0	Reference Year
R	Resistance, Universal Gas Constant in J/mol-K
k	Scaled Parameter
t	Scaled Year
u	Scaling Exponent
E^0	Standard Potential in V
T	Temperature in K
δ	Thickness in m
C_{TOC}	Total Overnight Capital in $

Abbreviations

AU	Air Utilization
AFOC	Annual Fixed Operating Cost
AVOC	Annual Variable Operating Cost
CO_2	Carbon Dioxide
CG	Coal Gasification
COE	Cost of Electricity
CAP	Criteria Air Pollutant
EPC	Engineering Procurement and Construction
FU	Fuel Utilization
GT	Gas Turbine
GHG	Greenhouse Gas
HAT	Humid Air Turbine
H_2	Hydrogen
ISO	International Organization for Standardization
LSCF	Lanthanum Strontium Cobalt Ferrite
LSM	Lanthanum Strontium Manganite
LCOE	Levelized Cost of Electricity
LHV	Lower Heating Value
NG	Natural Gas
NPV	Net Present Value
NiO	Nickel Oxide
PEN	Positive-electrode-electrolyte-negative-electrode
PR	Pressure Ratio
RH_2	Renewable Hydrogen
SOFC	Solid Oxide Fuel Cell
STIG	Steam Injection Generator
SMR	Steam Methane Reformation
ST	Steam Turbine/Rankine Cycle
TPC	Total Plant Cost
TIT	Turbine Inlet Temperature
YSZ	Yttria-Stabilized Zirconia

Appendix A

Table A1. Stream summary of the base case.

Stream Number	Unit	1	2	3	4	5	6	7	8
Temperature	°C	15	700	15	700	915	852	568	275
Pressure	bar	1.0	5.0	4.1	5	4.8	4.3	1.1	1.0
Mole Flowrate	kmol/h	2014	2014	218	218	218	2123	2123	2123
Mass Flowrate	kg/h	58,120	58,120	439	439	3332	58,559	58,559	58,559
Mass Vapor Fraction	-	1	1	1	1	1	1	1	1
Composition	mol-basis								
O_2	-	0.20741	0.20741	0.00000	0.00000	0.00000	0.14555	0.14555	0.14555
N_2	-	0.77315	0.77315	0.00000	0.00000	0.00000	0.73353	0.73353	0.73353
Ar	-	0.00924	0.00924	0.00000	0.00000	0.00000	0.00877	0.00877	0.00877
H_2	-	0.00000	0.00000	0.99986	0.99986	0.16858	0.00000	0.00000	0.00000
CO	-	0.00000	0.00000	0.00000	0.00000	0.00000	0.00000	0.00000	0.00000
CO_2	-	0.00033	0.00033	0.00000	0.00000	0.00000	0.00031	0.00031	0.00031
H_2O	-	0.00987	0.00987	0.00014	0.00014	0.83142	0.11184	0.11184	0.11184

Table A2. Stream summary of the cathode off-gas recirculation case.

Stream Number	Unit	1	2	3	4	5	6	7	8
Temperature	°C	15	700	15	700	917	1069	739	330
Pressure	bar	1.0	5.0	4.1	5.0	4.8	4.3	1.1	1.0
Mole Flowrate	kmol/h	1559	1997	218	218	218	1668	1668	1668
Mass Flowrate	kg/h	45,000	57,538	439	439	3331	45,439	45,439	45,439
Mass Vapor Fraction	-	1	1	1	1	1	1	1	1
Composition	mol-basis								
O_2	-	0.20741	0.19673	0.00000	0.00000	0.00000	0.12869	0.12869	0.12869
N_2	-	0.77315	0.78357	0.00000	0.00000	0.00000	0.72273	0.72273	0.72273
Ar	-	0.00924	0.00936	0.00000	0.00000	0.00000	0.00864	0.00864	0.00864
H_2	-	0.00000	0.00000	0.99986	0.99986	0.16883	0.00000	0.00000	0.00000
CO	-	0.00000	0.00000	0.00000	0.00000	0.00000	0.00000	0.00000	0.00000
CO_2	-	0.00033	0.00033	0.00000	0.00000	0.00000	0.00031	0.00031	0.00031
H_2O	-	0.00987	0.01000	0.00014	0.00014	0.83117	0.13963	0.13963	0.13963

Table A3. Stream summary of the anode off-gas recirculation case.

Stream Number	Unit	1	2	3	4	5	6	7	8
Temperature	°C	15	700	15	700	941	1103	754	312
Pressure	bar	1.0	5.0	4.1	5.0	4.8	4.6	1.1	1.0
Mole Flowrate	kmol/h	1473	1473	218	472	472	1582	1582	1582
Mass Flowrate	kg/h	42,500	42,500	439	4327	7213	42,939	42,939	42,939
Mass Vapor Fraction	-	1	1	1	1	1	1	1	1
Composition	mol-basis								
O_2	-	0.20741	0.20741	0.00000	0.00000	0.00000	0.12438	0.12438	0.12438
N_2	-	0.77315	0.77315	0.00000	0.00000	0.00000	0.71997	0.71997	0.71997
Ar	-	0.00924	0.00924	0.00000	0.00000	0.00000	0.00860	0.00860	0.00860
H_2	-	0.00000	0.00000	0.99986	0.55292	0.17080	0.00000	0.00000	0.00000
CO	-	0.00000	0.00000	0.00000	0.00000	0.00000	0.00000	0.00000	0.00000
CO_2	-	0.00033	0.00033	0.00000	0.00000	0.00000	0.00031	0.00031	0.00031
H_2O	-	0.00987	0.00987	0.00014	0.44708	0.82920	0.14673	0.14673	0.14673

References

1. Lai, W.-H.; Hsiao, C.-A.; Lee, C.-H.; Chyou, Y.-P.; Tsai, Y.-C. Experimental simulation on the integration of solid oxide fuel cell and micro-turbine generation system. *J. Power Sources* **2007**, *171*, 130–139.
2. O'Hayre, R.; Cha, S.-W.; Colella, W.; Prinz, F.B. *Fuel Cell Fundamentals*, 3rd ed.; John Wiley & Sons Inc.: Hoboken, NJ, USA, 2016.
3. Brouwer, J. Hybrid Gas Turbine Fuel Cell Systems. In *Gas Turbine Handbook*; Morgantown, W.V., Ed.; National Energy Technology Laboratory: Anchorage, AK, USA, 1982.
4. Veyo, S.E.; Lundberg, W.L.; Vora, S.D.; Litzinger, K.P. Tubular Sofc Hybrid Power System Status. In Proceedings of the ASME Turbo Expo 2003: Power for Land, Sea, and Air, Atlanta, GA, USA, 16–19 June 2003.

5. Smith, T.; Samuelsen, S.; Brouwer, J.; Hybrid—220KW Sofc/Micro Turbine Generator System. National Fuel Cell Research Center. Available online: http://www.apep.uci.edu/PDF_Archvied_Research_Summaries/HYBRIDfuelCELL_Hybrid_220kwSOFC.pdf. (accessed on 31 May 2022).
6. Huang, K.; Singhal, S.C. Cathode-supported tubular solid oxide fuel cell technology: A critical review. *J. Power Sources* **2013**, *237*, 84–97.
7. Willich, C.; Westner, C.; Seidler, S.; Leucht, F.; Henke, M.; Kallo, J.; Maier, U.; Friedrich, K.A. Pressurized Solid Oxide Fuel Cells: Operational Behavior. *Dtsch. Zent. Luft.* 2011. Available online: https://core.ac.uk/reader/11147430 (accessed on 22 May 2023).
8. Seidler, S.; Henke, M.; Kallo, J.; Bessler, W.G.; Maier, U.; Friedrich, K.A. Pressurized solid oxide fuel cells: Experimental studies and modeling. *J. Power Sources* **2011**, *196*, 7195–7202.
9. Gandiglio, M.; Lanzini, A.; Leone, P.; Santarelli, M.; Borchiellini, R. Thermoeconomic analysis of large solid oxide fuel cell plants: Atmospheric vs. pressurized performance. *Energy* **2013**, *55*, 142–155.
10. Rosner, F. Economics of cell design and thermal management in solid oxide fuel cells under SOFC-GT hybrid operating conditions: Part II, Pressure Dependency. *Res. Gate* **2021**.
11. Mueller, F.; Gaynor, R.; Auld, A.E.; Brouwer, J.; Jabbari, F.; Samuelsen, G.S. Synergistic integration of a gas turbine and solid oxide fuel cell for improved transient capability. *J. Power Sources* **2008**, *176*, 229–239.
12. Kang, S.; Ahn, K.Y. Dynamic modeling of solid oxide fuel cell and engine hybrid system for distributed power generation. *Appl. Energy* **2017**, *195*, 1086–1099.
13. Damo, U.M.; Ferrari, M.L.; Turan, A.; Massardo, A.F. Solid oxide fuel cell hybrid system: A detailed review of an environmentally clean and efficient source of energy. *Energy* **2019**, *168*, 235–246.
14. Rosner, F.; Rao, A.; Samuelsen, S. Thermo-economic analyses of solid oxide fuel cell-gas turbine hybrids considering thermal cell gradients. *J. Power Sources* **2021**, *507*, 230271.
15. Wang, X.; Lv, X.; Weng, Y. Performance analysis of a biogas-fueled SOFC/GT hybrid system integrated with anode-combustor exhaust gas recirculation loops. *Energy* **2020**, *197*, 117213.
16. Saebea, D.; Patcharavorachot, Y.; Assabumrungrat, S.; Arpornwichanop, A. Analysis of a pressurized solid oxide fuel cell–gas turbine hybrid power system with cathode gas recirculation. *Int. J. Hydrogen Energy* **2013**, *38*, 4748–4759.
17. Chen, J.; Li, J.; Zhou, D.; Zhang, H.; Weng, S. Control strategy design for a SOFC-GT hybrid system equipped with anode and cathode recirculation ejectors. *Appl. Therm. Eng.* **2018**, *132*, 67–79.
18. Cheddie, D.F. Integration of a solid oxide fuel cell into a 10 MW gas turbine power plant. *Energies* **2010**, *3*, 754–769.
19. Dawood, F.; Anda, M.; Shafiullah, G.M. Hydrogen production for energy: An overview. *Int. J. Hydrogen Energy* **2020**, *45*, 3847–3869.
20. He, W.; Abbas, Q.; Alharthi, M.; Mohsin, M.; Hanif, I.; Vo, X.V.; Taghizadeh-Hesary, F. Integration of renewable hydrogen in light-duty vehicle: Nexus between energy security and low carbon emission resources. *Int. J. Hydrogen Energy* **2020**, *45*, 27958–27968.
21. Alternative Fuels Data Center: Fuel Cell Electric Vehicle Emissions. Available online: https://afdc.energy.gov/vehicles/emissions_hydrogen.html (accessed on 30 March 2022).
22. Saeedmanesh, A.; Kinnon, M.A.M.; Brouwer, J. Hydrogen is essential for sustainability. *Curr. Opin. Electrochem.* **2018**, *12*, 166–181.
23. Ursúa, A.; Gandía, L.M.; Sanchis, P. Hydrogen production from water electrolysis: Current status and future trends. *Proc. IEEE* **2012**, *100*, 410–426.
24. Ayers, K.; Danilovic, N.; Ouimet, R.; Carmo, M.; Pivovar, B.; Bornstein, M. Perspectives on Low-Temperature Electrolysis and Potential for Renewable Hydrogen at Scale. *Annu. Rev. Chem. Biomol. Eng.* **2019**, *10*, 219–239.
25. Reed, J.; Dailey, E.; Shaffer, B.; Lane, B.; Flores, R.; Fong, A.; Samuelsen, G. Roadmap for the Deployment and Buildout of Renewable Hydrogen Production Plants in California. 2020. Available online: https://www.energy.ca.gov/publications/2020/roadmap-deployment-and-buildout-renewable-hydrogen-production-plants-california (accessed on 30 April 2023).
26. Hydrogen Shot | Department of Energy.
27. Chinda, P.; Brault, P. The hybrid solid oxide fuel cell (SOFC) and gas turbine (GT) systems steady state modeling. *Int. J. Hydrogen Energy* **2012**, *37*, 9237–9248.
28. Kuchonthara, P.; Bhattacharya, S.; Tsutsumi, A. Combinations of solid oxide fuel cell and several enhanced gas turbine cycles. *J. Power Sources* **2003**, *124*, 65–75.
29. Martinez, A.S.; Brouwer, J.; Samuelsen, G.S. Feasibility study for SOFC-GT hybrid locomotive power: Part I. Development of a dynamic 3.5 MW SOFC-GT FORTRAN model. *J. Power Sources* **2012**, *213*, 203–217.
30. David, M.; Bianchi, F.; Ocampo-Martinez, C.; Sánchez-Peña, R. H2 purity control of high-pressure alkaline electrolyzers. *IFAC-PapersOnLine* **2021**, *54*, 109–114.
31. Hanke-Rauschenbach, R.; Bensmann, B.; Millet, P. Hydrogen production using high-pressure electrolyzers. *Compend. Hydrog. Energy* **2015**, 179–224.
32. Los Angeles County | SoCalGas. Available online: https://www.socalgas.com/stay-safe/pipeline-and-storage-safety/natural-gas-pipeline-map/los-angeles (accessed on 24 June 2022).
33. Kopasz, J.P. Fuel cells and odorants for hydrogen. *Int. J. Hydrogen Energy* **2007**, *32*, 2527–2531.
34. Longden, T.; Beck, F.J.; Jotzo, F.; Andrews, R.; Prasad, M. Clean' hydrogen?—Comparing the emissions and costs of fossil fuel versus renewable electricity based hydrogen. *Appl. Energy* **2022**, *306*, 118145.

35. Hydrogen and Fuel Cell Technologies Office. Hydrogen Shot. Department of Energy. Available online: https://www.energy.gov/eere/fuelcells/hydrogen-shot. (accessed on 20 May 2023).
36. Satyapal, S.; Stetson, N.U.S. DOE Hydrogen Production Program & LAWE Meeting. In *US DOE Energy Earthshots*; 2022. Available online: https://www.hydrogen.energy.gov/pdfs/review22/plenary4_satyapal_2022_o.pdf (accessed on 30 April 2023).
37. Gotham, D.J.; Nderitu, D.G.; Giraldo, J.S.; Preckel, P.V. Natural Gas Market Study. 2013. Available online: https://www.purdue.edu/discoverypark/sufg/docs/publications/Natural%20Gas%20Market%20Study.pdf (accessed on 30 April 2023).
38. Li, M.; Powers, J.D.; Brouwer, J. A finite volume SOFC model for coal-based integrated gasification fuel cell systems analysis. *J. Fuel Cell Sci. Technol.* **2010**, *7*, 0410171–04101712.
39. Haji, S. Analytical Modeling of PEM Fuel Cell ieV Curve. 2010.
40. Noren, D.A.; Hoffman, M.A. Clarifying the Butler-Volmer equation and related approximations for calculating activation losses in solid oxide fuel cell models. *J. Power Sources* **2005**, *152*, 175–181.
41. Wen, Q.; Wu, Y.; Cao, D.; Zhao, L.; Sun, Q. Electricity generation and modeling of microbial fuel cell from continuous beer brewery wastewater. *Bioresour. Technol.* **2009**, *100*, 4171–4175.
42. Battelle Memorial Institute. *Manufacturing Cost Analysis of 100 and 250 kW Fuel Cell Systems for Primary Power and Combined Heat and Power Applications*; Battelle Memorial Institute: Columbus, OH, USA, 2016.
43. Rosner, F.; Yang, D.; Rao, A.; Samuelsen, S. Technical note: Gas turbine price projection for n-th plant equipment cost. *Eng. Econ.* **2022**, *67*, 325–330.
44. Van Eeden, P.; Ercolani, D. A Method for Prediction of Gas/Gas Ejector Performance. *Impiantistica Ital.* 2013, pp. 75–80. Available online: https://www.semanticscholar.org/paper/A-Method-for-Prediction-of-Gas-Gas-Ejector-Eeden-Ercolani/37cf6b47ceade8bfe4c2779c5efaea86b3a12c84#citing-papers (accessed on 29 April 2023).
45. Lukas, M.D.; Ghezel-Ayagh, H.; Sanderson, R.; Krishnan, S. Development of a Microchannel High Temperature Recuperator for Ultra-High Efficiency Fuel Cell/Turbine Systems. *ECS Trans.* **2012**, *42*, 267–271.
46. Iyengar, A.K.S.; Newby, R.A.; Keairns, D.L. *Techno-Economic Analysis of Integrated Gasification Fuel Cell Systems*; Created by Energy Sector Planning and Analysis for SEAP & OPPB Office of Fossil Energy; National Energy Technology Laboratory (NETL): Pittsburgh, PA, USA, 2014.
47. Rosner, F. *PhD thesis Design and Thermo-Economic Analyses of Solid Oxide Fuel Cell-Gas Turbine Hybrid Systems with Water Recovery*; University of California: Irvine, CA, USA, 2021.
48. Rosner, F.; Rao, A.; Samuelsen, S. Economics of cell design and thermal management in solid oxide fuel cells under SOFC-GT hybrid operating conditions. *Energy Convers. Manag.* **2020**, *220*, 112952.
49. DOE/NETL. Techno-Economic Analysis of Integrated Gasification Fuel Cell Systems. 2014.
50. Bohn, D. Micro Gas Turbine and Fuel Cell—A Hybrid Energy Conversion System with High Potential. 2005.
51. Biswas, N.; Bhattacharya, D.; Kumar, M.; Mukhopadhyay, J.; Basu, R.N.; Das, P.K. Effect of Oxygen Diffusion Constraints on the Performance of Planar Solid Oxide Fuel Cells for Variable Oxygen Concentration. *Ind. Eng. Chem. Res.* **2020**, *59*, 18844–18856.